Solar Energy Materials & Solar Cells 117 (2013) 120–125

Contents lists available at ScienceDirect

Solar Energy Materials & Solar Cells

journal homepage: www.elsevier.com/locate/solmat

Optimized short-circuit current mismatch in multi-junction solar cells

M. Bonnet-Eymard *, M. Boccard, G. Bugnon, F. Sculati-Meillaud, M. Despeisse, C. Ballif

Photovoltaics and thin film electronics laboratory (PV-Lab), Institute of Micro-engineering (IMT), Ecole Polytechnique Fédérale de Lausanne (EPFL), Rue Breguet 2, 2000 Neuchatel, Switzerland

ARTICLE INFO

Article history:
Received 19 February 2013
Received in revised form
15 May 2013
Accepted 21 May 2013
Available online 19 June 2013

Keywords:
Multi-junction photovoltaic devices
Current–Voltage measurements
Irradiance spectrum
Current matching
Thin-film silicon

ABSTRACT

Multi-junction photovoltaic devices include two or more component sub-cells which are electrically interconnected in series. At any power point, the current output of the total device is limited by the sub-cell with the smallest current density. Therefore, the maximum efficiency is reached when the sub-cells have equal current densities at their respective maximum power points. In this case the sub-cells are so called "power matched". We report an experimental procedure in which the current–voltage characteristics of tandem solar cells can be measured under various irradiance spectra, i.e. under various short-circuit current matching conditions. This permits the probing of the optimized short circuit current mismatch, where the sub-cells are power matched, which is essential to define design rules for the tandem stack. The method applies well to devices where one of the sub-cells is metastable. We show that, in the case of thin-film silicon tandem cells, the optimum mismatch changes significantly after light induced degradation. Consequently, the degradation factor of such devices is shown to depend not only on material quality but also on the initial short circuit current matching. This experiment also provides relative quantification of the fill factors of each sub-cell. Our example suggests that a high bottom cell deposition rate can be detrimental to the fill factor of the top cell in the case of thin-film silicon tandem cells deposited in superstrate configuration.

1. Introduction

Stacking solar cells with materials of different band gaps reduces thermalization losses and therefore increases the efficiency limit of a photovoltaic device [1]. In such multi-junction configurations, the sub-cells can be electrically connected in series. This implies that, at a given power point, the sub-cell with the smallest current density will limit the current density of the whole device. To maximize the power conversion efficiency, the sub-cells should have equal current densities at their respective maximum power point (MPP), this current density being then the MPP current density of the multi-junction device [2]. This so-called "power matching" condition [3] differs from the short-circuit current (J_{SC}) matching condition, unless the current–voltage (I–V) characteristics of the sub-cells are identical [4]. In thin film multi-junction devices, one sub-cell can exhibit meta-stability effects, which makes the device optimization for stabilized-state operation more difficult.

In the case of micromorph tandem cells, a high band gap (1.6–1.8 eV) hydrogenated amorphous silicon (a-Si:H) top cell is combined with a low band gap (1.1 eV) microcrystalline silicon (μc-Si:H) bottom cell. Because of the top cell light induced degradation (LID) known as the Staebler–Wronski effect [5], this sub-cell usually has a lower fill factor than the bottom cell after stabilization. Consequently, in this configuration simulations [6] have shown that the current of the total device should be slightly limited by the bottom cell, in short circuit condition, to reach power matching and thus maximize the efficiency. It should be noted that this optimization should be made according to the irradiance spectrum.

The balance of photocurrent between the sub-cells can be tuned by changing the thickness of the a-Si:H and μc-Si:H layers or, more advantageously, by using intermediate reflectors based on zinc oxide (ZnO) [7] or silicon oxide (SiO_x) [8]. The J_{SC} of each sub-cell is easily obtained by the measurement of separated external quantum efficiencies (EQE) [9]. J_{SC} matching is therefore straightforward to evaluate. However, probing the power matching requires either the complete I–V curve of the sub-cells [10], or the measurement of the total device efficiency under different irradiance spectra while keeping the same total current in the tandem device [3].

In this paper, we use a method similar to [3] in order to determine the optimal J_{SC} mismatch of micromorph devices with different top and bottom cell performances, before and after LID, i.e. after 1000 h of light soaking under 1 Sun. After introducing the "current matching" apparatus and the calculations involved, we

* Corresponding author. Tel.: +41 32 718 33 24.
E-mail address: maxbonneteymard@gmail.com (M. Bonnet-Eymard).

0927-0248/$ - see front matter © 2013 Elsevier B.V. All rights reserved.
http://dx.doi.org/10.1016/j.solmat.2013.05.046

present a sample series where we have varied the electrical quality of both sub-cells by using different substrate roughnesses and bottom-cell material qualities, obtained through varying the deposition rate. Then, the *I–V* parameters of the sample series are plotted as a function of the short-circuit current matching of the sub-cells. Finally, we discuss the impact of these series parameters on the performance of each sub-cell and its effect on the optimized J_{SC} mismatch. Our experimental data is supported with simulated results obtained from an equivalent network model.

2. Experiment

2.1. Current matching set-up

Illuminated *I–V* measurements are performed under a class AAA Wacom solar simulator (WXS-220S-L2 AM1.5G) following the Standard Test Conditions (STC). The irradiance spectrum is therefore close to AM 1.5G with an irradiance intensity of 1000 W/m^2 (1 Sun). To study micromorph devices in the degraded state, light soaking for 1000 h is done using a Solaronix system with an irradiance intensity of 1 Sun.

In this experiment, *I–V* curves of micromorph tandem cells are measured under an intentionally modified irradiance spectrum, in order to artificially change the current matching condition of the tandem device. The sum of the J_{SC} of the sub-cells (hereon referred to as "total current") is kept constant; only the ratio of the top and the bottom sub-cell J_{SC} varies. Consequently, the number of incident photon is kept constant but not the irradiance power density. Therefore, we will consider in the following the power output of the devices and not their efficiency.

We refer to the set-up that enables us to modify the spectrum as the "current matching machine" (CMM). The CMM set-up is illustrated in Fig. 1: the intensity of the AM 1.5 STC spectrum irradiance is reduced by 15% thanks to the reflection of two tilted glass slides. The attenuation is homogenous between 370 and 1100 nm. To compensate for this irradiance reduction, the light intensity corresponding to 15% of the total current of the tandem device is added and redistributed to the top and the bottom cells with two dedicated light sources. The balance of current distribution between the top and the bottom sub-cell can be tuned by adjusting the power of each selective light source. In the case of micromorph devices, we use monochromatic LEDs emitting at 470 and 870 nm for excitation of the top and bottom cells respectively. This experiment could be applied to other types of multi-junction devices by adapting the selective light biases.

The LED's electronic power is controlled by in-house electronics and a National Instruments USB-6009 acquisition card. The LEDs optical power is calibrated using a Hamamatsu photodiode with known EQE. The relative emission spectra of the LEDs are measured with an Arcoptics spectrometer. The EQE of the sub-cells is measured with an apparatus similar to that described in [8].

The electronic power needed from the blue LEDs to obtain the desired top-cell current is given by

$$Pwr_{B_{LED}}(J_{scT}) = \frac{\int[(QE_{top}(\lambda)/QE_{ref}(\lambda))B_{spec}(\lambda)]}{B_{spec}(\lambda)} Pwr_{B_{LED}}(J_{sc\ ph}), \quad (1)$$

where $Pwr_{B_{LED}}$ is the optical power of the blue LEDs, J_{scT} is the short-circuit current in the top cell, λ is the wavelength, B_{spec} is the spectrum of the blue LEDs, $J_{sc\ ph}$ is the J_{SC} of the reference Hamamatsu photodiode, QE_{top} and QE_{ref} are the quantum efficiencies of the top cell and reference photodiode respectively.

The same calculation applies for the red LEDs and the bottom cell. According to these calculations, a sub-cell-specific calibration is made. First, one sub-cell is saturated by increasing its J_{SC} by 5 mA/cm^2, so that the other subcell limits the current; then, the J_{SC} of the limiting sub-cell is increased by steps of 0.5 mA/cm^2. Consequently, the J_{SC} of the total device should increase at each step by 0.5 mA/cm^2. The mean of actual J_{SC} increase in the total device is used to correct the calculated electronic power in the LED needed to obtain the desired current in each sub-cell.

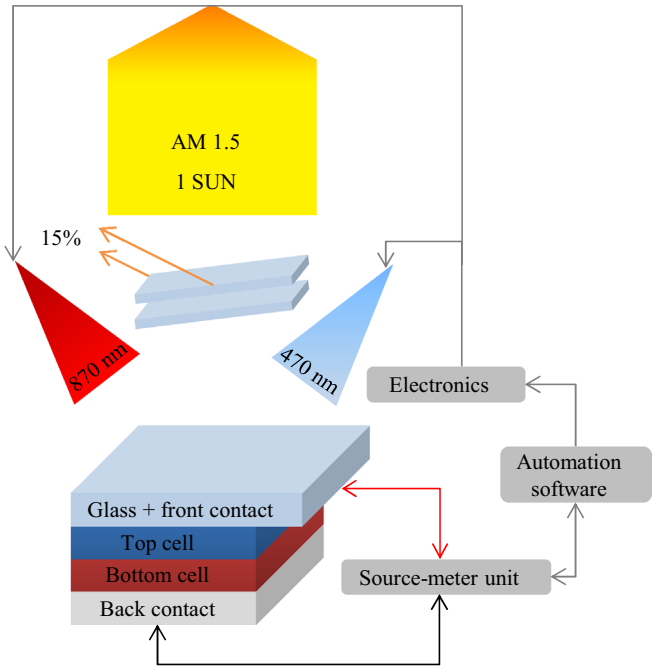

Fig. 1. Sketch of the current-matching-machine experimental set-up. It aims at measuring *I–V* curves under various irradiance spectra. 15% of the intensity of the STC AM 1.5G spectrum irradiance is removed thanks to two glass slides. The decrease in total current is compensated with monochromatic LEDs in order to keep the total current constant. The blue (470 nm) and red (870 nm) LEDs permit tuning of the photocurrent of the top and bottom cells respectively.

2.2. Measurement procedure

After these sub-cell-specific calibrations, we define an array of J_{SC} matching conditions for illuminated *I–V* measurements (typically 8 points). J_{SC} matching conditions are here on referred to as J_M and given by

$$J_M = (J_{EQE\_top} - J_{EQE\_bot}) + (J_{ad\_top} - J_{ad\_bot}), \quad (2)$$

where J_{EQE_top} and J_{EQE_bot} are respectively the J_{SC} of the top and bottom cells calculated from EQE measurement and J_{ad_top} and J_{ad_bot} are respectively the photocurrent added in the top and the bottom cell thanks to the two selective LEDs sets.

The chosen J_M are restrained by the fact that only 15% of the total current can be redistributed. We calculate, for each J_M, the corresponding additional photocurrent needed for the top and bottom sub-cells, and according to formula (1), the corresponding blue and red LED power required. The power required is then corrected using the sub-cell-specific calibration. After performing *I–V* measurements under the different spectral conditions, we get plots of each tandem cell *I–V* parameters with respect to J_M. The maximum J_{SC} of the tandem device is obtained at short circuit current matching of the sub-cells (J_M=0 mA/cm^2). The maximum power output is reached at power matching. The calibration and *I–V* measurement steps are fully automated and performed in less than 5 min for one device under test.

2.3. Sample series

In this work, the CMM set-up is used to study a series of micromorph devices in the superstrate configuration (p-i-n). In such configuration, the a-Si:H top cell is deposited first, followed by the μc-Si:H bottom cell. Therefore, deposition conditions (e.g temperature, power) of the bottom cell can possibly affect the top cell quality. The devices were co-deposited on boron doped zinc oxide (ZnO:B) grown by Low Pressure Chemical Vapor Deposition (LPCVD) with two plasma post-deposition treatments. Such post-deposition treatment is used to smooth the native random pyramids, of which the height and sharpness directly affect the *IV* parameters of both the top and bottom cells. A rougher substrate is expected to favor light trapping, and boost the J_{SC} [11]; However, it is usually associated with a decrease of the fill factor (*FF*) and open-circuit voltage (V_{OC}), as it induces structural defects in the materials with the formation of nanoporous regions [12,13]. In the sample series presented here, 2 μm thick ZnO:B substrates were plasma treated for 4 and 16 min to obtain relatively "rough" and "smooth" morphologies respectively. For each substrate, bottom cells were deposited at two deposition rates of 3 and 15 Å/s. Increasing μc-Si:H deposition rate deteriorates the electrical quality of the sub-cell due to both increased bulk defect density and nanoporous region formation [14]. The goal of this study is to evaluate the impact of the roughness of the substrate and the deposition rate of the μc-Si:H material on the performance of the sub-cells and, consequently, on the optimized short circuit current mismatch (i.e. power matching) of the tandem devices.

3. Results and discussion

3.1. Open circuit voltage

Table 1 shows the V_{OC}'s of the complete sample series at J_M=0 mA/cm^2. V_{OC} versus matching condition is almost constant (not shown) and the observed differences are attributed to temperature variations (< 5 mV without specific trend). As expected, for reasons described in the previous section, devices deposited on smooth substrates exhibit higher V_{OC}. According to V_{OC} measurement on single junction reference devices (see table 2), the V_{OC} gain with a smooth substrate is due to an improvement in both sub-cells. Furthermore, devices with a bottom cell deposited at low rate (LR) exhibit higher V_{OC} than those with a high rate (HR) bottom cell. This V_{OC} increase is supposedly gained mostly from the bottom cell because of improvement of its i-layer material quality.

3.2. Power output: probing the optimal J_{SC} mismatch

Fig. 2 shows the evolution of the power output versus J_{SC} mismatch (J_M) obtained with the CMM set-up. This plot permits comparison of the performance of different device designs even if they do not have the same original J_{SC} mismatch.

Table 1
Open-circuit voltages of micromorph tandem devices under the short-circuit current matching condition with bottom cells deposited at high (HR) and low (LR) rate, using smooth and rough substrate, in initial and degraded states.

Bottom cell dep. rate	Substrate	V_{OC} initial [mV]	Voc degraded [mV]
HR	Smooth	1358	1348
	Rough	1332	1315
LR	Smooth	1424	1395
	Rough	1402	1386

Table 2
Open-circuit voltages of corresponding a-Si:H and μc-Si:H single junction reference cells deposited on smooth or rough substrates. Bottom cells are deposited at high (HR) or low (LR) rate.

Substrate	a-Si:H	V_{OC} single cell [mV]	
		Deposition rate	μc-Si:H
Rough	901	HR	459
		LR	514
Smooth	913	HR	474
		LR	527

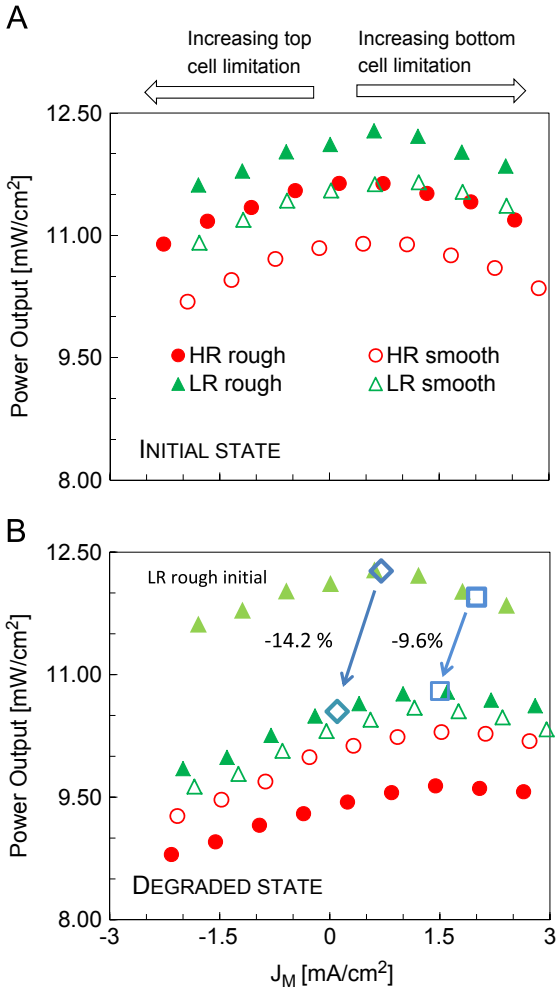

Fig. 2. Power output versus short-circuit current matching (J_M) obtained from *I–V* measurements done under various irradiance spectra. The number of incident photon is kept constant but not the irradiance power density which is why we plot the power output and not the efficiency. Power output in mW/cm^2 is equivalent to efficiency in % if the irradiance intensity is 100 mW/cm^2 (AM 1.5G). a and b show measured cell power output for initial and degraded state respectively. HR and LR stands for high and low bottom cell deposition rate, respectively. The "rough" and "smooth" terms refer to the two types of substrate roughness. In b, the diamonds and the squares show the evolution of the power output after degradation for two initial J_{SC} matching conditions of the same device.

In initial state, (Fig. 2a) devices with smooth substrates exhibit lower power output than their equivalent device with rough substrate. This is because the rough substrate improves the light trapping and strongly increases the photo-generated current in the sub-cells [15]. Also, when going from HR to LR bottom cell devices, an improvement in power output is observed due to increased V_{OC} and *FF*. The maximum power output, corresponding

to the power matching between the top and bottom sub-cells, is reached for a J_{SC} mismatch around J_M=0.5 mA/cm^2 i.e. under slightly bottom limited condition. There are two reasons for this: firstly, the fill factor (*FF*) of the bottom cell is generally slightly higher than that of the top cell, due to better collection efficiency. Secondly, the higher V_{OC} of the top cell leads to a higher FF of the total device under the bottom limited condition compared to the top limited condition, even for equal sub-cell FF. Overall, in initial state, despite the device design differences, the optimal J_{SC} mismatch is very similar for all cells.

After degradation (Fig. 2b), all power output curves shift down, but not by the same amount. The rough-substrate devices degrade more than the smooth-substrate ones. In the case of HR bottom cell devices, the gain in current from a rough substrate is overtaken by the loss in V_{OC} and FF, whereas for LR bottom cell devices both substrates yield similar power output after degradation. Furthermore, the optimized J_{SC} mismatch of all devices is shifted to an increased bottom cell short-circuit current limitation condition: around J_M=1.5 mA/cm^2. This is due to the strong FF decrease (about 10% absolute is expected) of the top cell due to LID. It should also be noted that the current produced by the top cell decreases typically by about 0.5 mA/cm^2 during LID for the 250 nm thick cell employed, changing the short circuit current matching of the device under AM 1.5G.

This CMM study on power output shows that the different device design parameters employed do not drastically impact the optimum J_{SC} mismatch. However, this optimum changes significantly after light soaking, demonstrating that the degradation factor depends on the initial short-circuit current matching: if the micromorph design is optimized in order to reach power matching in the initial state, one will get a strong degradation factor and no optimized J_{SC} mismatch after degradation. For example, in the series tested, the degradation would have been in this case, 14.2% (see diamonds in Fig. 2b). However, if the device was designed so that the short-circuit current matching was strongly bottom cell limited (in the series tested, J_M=2 mA/cm^2), after degradation we would get J_M=1.5 mA/cm^2, i.e. power matching and therefore a maximized stabilized power output. In this case, the degradation factor is then reduced to 9.6% after LID (see empty squares in Fig. 2b). This emphasizes the need for high top-cell current to reach high stable efficiency in micromorph devices. For that purpose, efficient selective intermediate reflectors are mandatory. This study also clearly shows that the power output degradation depends not only on material quality (a-Si:H cell sensitivity to Staebler–Wronski effect), but also on the initial matching condition. The degradation factor (in %) of a micromorph solar cell is an imprecise assessment of the material quality itself. As shown, by varying the matching in otherwise similar cells, the power output degradation can vary from 9.6 to 14.2%.

3.3. Fill factor: device design and the role of fabrication parameters

3.3.1. Experimental

Fig. 3 shows the evolution of the fill factor (*FF*) versus J_{SC} mismatch (J_M). With the CMM measurements, one can easily compare *FF* of different tandem devices even without the same actual current matching: the set-up permits decoupling the cell electrical performance from the tandem cell matching condition.

As explained in [16], the more one sub-cell is limiting the current, the more the *FF* of the total device reflects that of the limiting sub-cell. Therefore, the extreme values of the curves reflect the *FF* of the top cell (J_M=−3 mA/cm^2) and the bottom cell (J_M=3 mA/cm^2).

In initial state, shown in Fig. 3a, the FF difference between devices deposited on smooth and rough substrates is small and only visible in the bottom limited region. This indicates that the substrate roughness affects mostly the *FF* of the bottom cell. The difference in *FF* curves between devices including either a HR or LR bottom cell is more significant and is not limited to the bottom limited region. It seems to indicate that the bottom-cell deposition rate does not only affect the bottom cell performance.

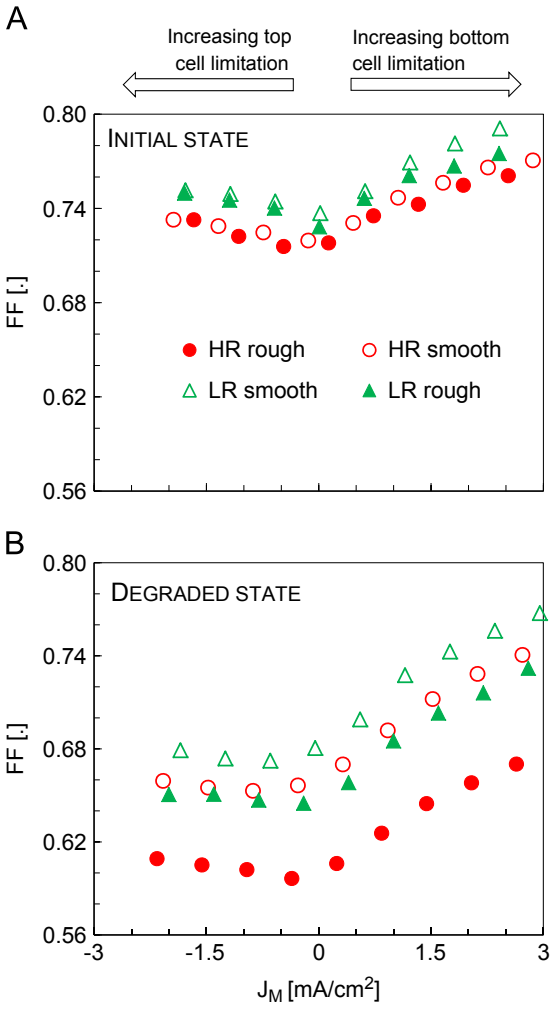

Fig. 3. Fill factor versus short circuit current matching (J_M) obtained by *I–V* measurement under various irradiance spectra. Fig. 2a and b show measured FF for initial and degraded cells respectively. HR and LR stands for high and low bottom cell deposition rate respectively. "rough" and "smooth" define the two types of substrate roughness.

In degraded state (Fig. 3b), the *FF* curves have a modified shape compared to those in initial state: the top limited side is flatter and the bottom limited side steeper. This is because light soaking principally affects the a-Si:H top cell performance: its *FF* is expected to decrease by 10% absolute. Furthermore, we see that the *FF* curves shift downward, but not by the same amount, similar to the power output curves.

In order to better understand the changes in the *FF* curves induced by light soaking, simulation calculations are presented in the following section.

3.3.2. Simulations

We have simulated *I–V* curves of a tandem device under various short circuit current matching conditions. For this purpose, the simulated photocurrent balance between the top and the bottom cell has been varied. We used an equivalent network model based on the one developed by Merten [17] for thin-film silicon solar

cells. The *FF*s were calculated and plotted versus J_M for different quality parameters of the top and the bottom cells.

In Fig. 4a, b and c is plotted the *FF* curve obtained with the reference parameters proposed for the model employed in [6] for an initial state micromorph device. In Fig. 4a and b, the *FF*s of the top and the bottom sub-cells have been improved or decreased separately using two different parameters of the model: the mobility-lifetime product ($\mu\tau$) and the diode quality. The diode quality is defined by the saturation current J_0 and the ideality factor n. These parameters have been changed in order to modify the *FF* of a sub-cell while maintaining the total V_{OC} plausible,

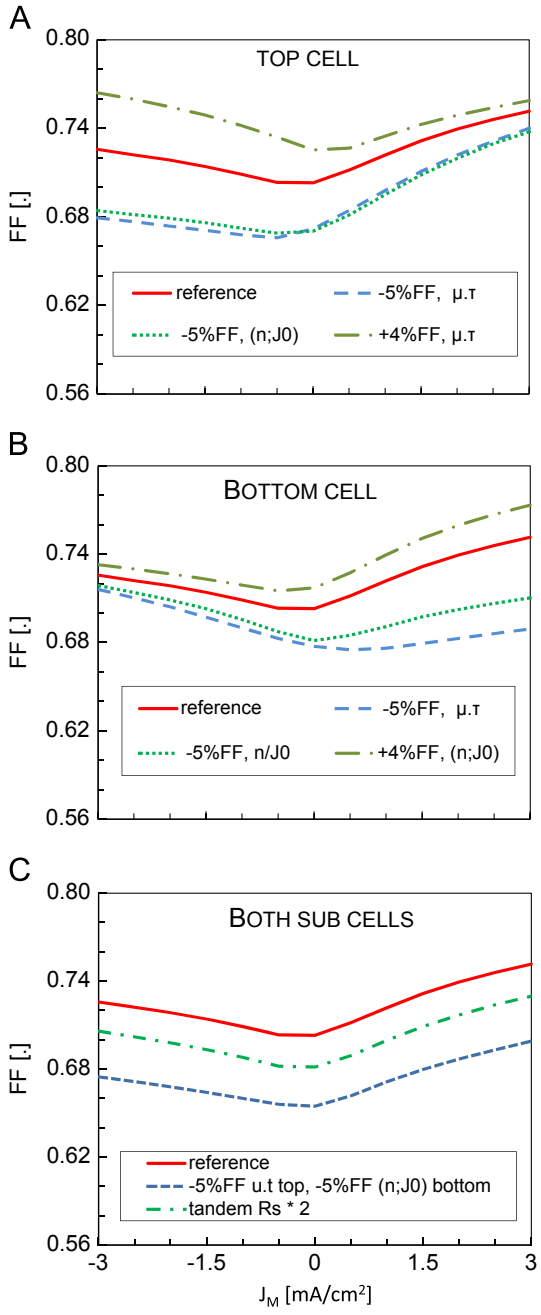

Fig. 4. Fill Factors obtained from simulated *I–V* curves using an equivalent network model. The short circuit current matching of the sub-cells has been varied by changing the photocurrent in each sub-cell. The different curves represent the results obtained with varied mobility-lifetime product ($\mu\tau$) and diode quality (n; J_0) in one or the other sub-cell. In c, both sub-cell's FF are modified as well as the series resistance (R_S) of the complete device. (For interpretation of the references to color in this figure, the reader is referred to the web version of this article.)

in respect of the obtained experimental values. In Fig. 4c, we combine degradation of *FF* of both sub-cells, and modify the series resistance (R_S) of the total device. The total device open-circuit resistance (R_{OC}) of the sample series, measured with standard *I–V* measurements increases from 12+/−1 Ω.cm^2 in initial state to 16+/−2 Ω.cm^2 in degraded state regardless of the device design. In the simulation, R_S has been doubled in order to match the range of R_{OC} variation obtained experimentally.

Undoubtedly, changing the parameters of one sub-cell mainly affects the side of the FF curve where this sub-cell is limiting the current. In Fig. 4a, the blue curve corresponds to a decrease of the top-cell FF by 5% due to a reduction of the $\mu\tau$ product in the model. This is the typical shape obtained experimentally after degradation in Fig. 3b. This confirms that mainly the top cell loses performance during LID. Considering Fig. 4c, one can see that combining the FF decrease in both sub-cells and modifying the R_S of the total device, results in FF curves keeping the same shape. Therefore, it is probable that the increased degradation factor when combining HR bottom cell and rough substrate is a joint effect due to R_S increase and degradation of both top and bottom cells. Considering the bottom cell, the rough substrate combined with high deposition rate is known to increase nanoporous region formation. This can lead to further degradation over time from water vapor ingress (our experimental devices are not encapsulated), and to an increased dark saturation current [15,18]. This degradation mechanism is not light induced and could also affect the intermediate reflector of the micromorph device, leading to an R_S increase. Considering the top cell, there are several possibilities that could explain a stronger FF degradation for devices deposited on rough substrates that include a HR bottom cell: Firstly, the HR bottom cell micro-cracks could act as paths for humidity and in-diffusion of atmospheric gases, eventually damaging the top cell. Secondly, the temperature elevation induced by the higher power density required for the HR bottom cell deposition could be detrimental to the top cell too. This detrimental effect would be amplified during light soaking. To verify these hypotheses, further experiments would be necessary.

Finally, this tool is useful for investigating if a difference in FF between two device designs should be attributed to one or the other sub-cell. From our study it seems that there is a combination of several effects including increased R_S and *FF* degradation of both sub-cells.

4. Conclusion

In this contribution, we have presented a technique that enables the modification of the irradiance spectrum to measure *I–V* curves of tandem cells under different short-circuit current matching conditions. This technique permits the probing of the optimal J_{SC} mismatch, where the energy conversion efficiency is maximal. In the case of micromorph tandem cells, experimental results show that J_{SC} mismatch should not be optimized in the initial state because it will shift after light induced degradation. For the micromorph devices employed, a strong (2 mA/cm^2) short-circuit current mismatch where the bottom cell is limiting the current leads to power matching after LID. This demonstrates the need for high current in the top cell and therefore efficient selective intermediate reflectors in thin film silicon tandem solar cells to maximize stable efficiency. The developed tool can help set design rules for tandem devices; beyond that, it gives valuable information on the fill factors of each sub-cell. Indeed, in the range of our experiment, we observed that the bottom cell deposition rate possibly affects the *FF* of the degraded top cell in superstrate configuration. The presented characterization technique can also be up-scaled to the module size, for instance using the advanced

LED/halogen hybrid large area solar simulator developed in our laboratory [19].

Acknowledgments

The authors would like to thank the Swiss federal office of energy (OFEN) for financial support, Johannes Seif for precious help concerning the simulations and Christian Schlumpf for proof reading the manuscript.

References

[1] C.H. Henry, Limiting efficiencies of ideal single and multiple energy gap terrestrial solar cells, Journal of Applied Physics 51 (1980) 4494–4500.
[2] T. Repmann, et al., Investigations on the current matching of highly efficient tandem solar cells based on amorphous and microcrystalline silicon, in: Proceedings of the 3rd WCPEC 2, 2003, vol. 1, pp. 1843–1846.
[3] C. Ulbrich et al., Power matching of tandem solar cells, in: Proceedings of the 26th EU PVSEC, 2011, vol. 1, pp. 302–305.
[4] R. Platz, Amorphous silicon for optimized multi-junction solar cells: material study and cell design, Université de Neuchâtel, Switzerland, 1999. (Ph.D. thesis), pp. 91-95.
[5] D.L. Staebler, C.R. Wronski, Reversible conductivity changes in discharge-produced amorphous Si, Applied Physics Letters 31 (1977) 292–294.
[6] D. Dominé, The role of front electrodes and intermediate reflectors in the optoelectronic properties of high-efficiency micromorph solar cells, Université de Neuchâtel, Switzerland, 2009. (Ph.D. thesis), pp. 107–115.
[7] R. Biron, et al., New progress in the fabrication of n–i–p micromorph solar cells for opaque substrates, Solar Energy Materials and Solar Cells 114 (2013) 147–155.
[8] P. Buehlmann, et al., In situ silicon oxide based intermediate reflector for thin-film silicon micromorph solar cells, Applied Physics Letters 91 (2007) 143–505.
[9] J. Burdick, T. Glatfelter, Spectral response and *I–V* measurements of tandem amorphous-silicon alloy solar cells, Solar Cells 18 (1986) 301–314.
[10] J. Holovský, et al., Variable light biasing method to measure component I–V characteristics of multi-junction solar cells, Solar Energy Material and Solar Cells 103 (2012) 128–133.
[11] M. Boccard, et al., Optimization of ZnO front electrodes for high-efficiency micromorph thin-film Si solar cells, IEEE Journal of Photovoltaics 2 (2012) 229–235.
[12] M. Python, et al., Relation between substrate surface morphology and microcrystalline silicon solar cell performance, Journal of Non-Crystalline Solids 354 (2008) 19–25.
[13] Nasuno, et al., Effects of substrate surface morphology on microcrystalline silicon solar cells, Japanese Journal of Applied Physics 40 (2001) 303.
[14] G. Bugnon, et al., A new view of microcrystalline silicon: the role of plasma processing in achieving a dense and stable absorber material for photovoltaic applications, Advanced Functional Materials 22 (2012) 3665–3671.
[15] Sai, et al., Impact of front and rear texture of thin-film microcrystalline silicon solar cells on their light trapping properties, Journal of Applied Physics 108 (2010) 044505.
[16] B. Yan et al., Correlation of current mismatch and fill factor in amorphous and nanocrystalline silicon based high efficiency multi-junction solar cells, in: Proceedings of the 33rd IEEE PVSC, 2008, vol. 1, pp. 1–6.
[17] J. Merten, et al., Improved equivalent circuit and analytical model for amorphous silicon solar cells and modules, IEEE Transaction on Electron Devices 45 (1998) 423–429.
[18] M. Boccard, et al., Substrate dependent stability and interplay between optical and electrical properties in μc-Si:H single junction solar cells, Solar Energy Materials and Solar Cells 95 (2011) 195–198.
[19] A. Lo et al., An hybrid LED/Halogen large-area solar simulator allowing for variable spectrum and variable illumination pulse shape, in: Proceedings of the 25th EU-PVSEC, Valencia, Spain, 2010.